Li3SbO4 lithium-ion battery material: Defects, lithium ion diffusion and tetravalent dopants

Kuganathan, N., Kordatos, A., Anurakavan, S., Iyngaran, P. & Chroneos, A.

Original citation & hyperlink:
Kuganathan, N, Kordatos, A, Anurakavan, S, Iyngaran, P & Chroneos, A 2019, 'Li3SbO4 lithium-ion battery material: Defects, lithium ion diffusion and tetravalent dopants' Materials Chemistry and Physics, vol. 225, pp. 34-41.
https://dx.doi.org/10.1016/j.matchemphys.2018.12.055

DOI 10.1016/j.matchemphys.2018.12.055
ISSN 0254-0584

Publisher: Elsevier

Li_3SbO_4 Lithium-Ion Battery Material: Defects, Lithium Ion Diffusion and Tetravalent Dopants

Navaratnarajah Kuganathan,[1,a] Apostolos Kordatos,[2] Sripathmanathan Anurakavan[3], Poobalasuntharam Iyngaran[3] and Alexander Chroneos[1,2,b)]

[1]Department of Materials, Imperial College London, London, SW7 2AZ, United Kingdom

[2]Faculty of Engineering, Environment and Computing, Coventry University, Priory Street, Coventry CV1 5FB, United Kingdom

[3] Department of Chemistry, University of Jaffna, Sir. Pon Ramanathan Road, Thirunelvely, Jaffna, Srilanka

---

Lithium antimony oxide, Li_3SbO_4, is a candidate anode material for rechargeable lithium ion batteries. Static atomistic scale simulations based on the classical pair potentials are employed to provide insights into the defect chemistry, doping behaviour and lithium diffusion paths in Li_3SbO_4. Here we show that, Li Frenkel is the dominant intrinsic defect process and the activation energy of Li diffusion is very low (0.21eV) suggesting that very high Li conduction is expected in this material. In particular, long range lithium diffusion paths *via* vacancy mechanism were constructed and it is confirmed that the lowest activation energy migration path is along the *bc*-axis plane with a zig-zag pattern. The calculations further suggest that cation anti-site defects, in which Li and Sb exchange their atomic positions, would not be observed with significant intrinsic concentration at operating temperatures. Subvalent doping by Si on the Sb site is energetically favourable suggesting that this efficient way to increase the Li content in Li_3SbO_4 should be stimulated experimentally. The electronic structure calculations based on the density functional theory (DFT) show that introduction of tetravalent dopants will not alter the band-gap significantly.

Keywords: Li_3SbO_4; Defects; Li diffusion; Dopants

[1]Corresponding authors, e-mails: a) n.kuganathan@imperial.ac.uk ; b) alexander.chroneos@imperial.ac.uk

1. Introduction

As there is an ever increasing requirement for reliable electrical energy storage for mobile applications (i.e. laptops and smart phones) there is demand for solid-state Li-ion batteries with high energy densities [1-22]. The development of materials is focused on the high-capacity electrode materials and electrolytes and such materials require high Li^+ ion concentration, low cost, less hazard and its constituent elements being high abundance. As there is no potential breakthrough in producing high capacity batteries, active research is still being continued in the discovery of promising electrode materials.

In recent years, lithium-excess compounds, Li_3MO_4 (M=Ru, Nb, Sb and Ta), have attracted considerable interest due to their anionic redox performance and ability to host many Li^+ ions leading to the formation of high capacity Li battery materials required for the development of electrical vehicles and consumer electronics.[23] "Li-rich" Li_3SbO_4 was experimentally studied as a high rate anode material with high power density due to its excellent rate performance, cycleability and excellent Coulombic efficiency though a low average reversible capacity of 81 $mAhg^{-1}$ is observed and a Li de-intercalation potential of 1.05 eV [24]. Furthermore, a theoretical capacity of 259.5 $mAhg^{-1}$ is expected with the possible reduction of Sb from +5 to +3. As there is an accessible capacity of 73 $mAhg^{-1}$ at a charge-discharge rate of 43 C and there is no significant fading observed after 200 cycles, Li_3SbO_4 was used to synthesize nanocrystalline composites ($Li_4Ti_5O_{12}/Li_3SbO_4/C$) anodes to improve the capacity of pristine $Li_4Ti_5O_{12}$[25]. Furthermore, monoclinic crystal structure of Li_3SbO_4 is expected to host excess Li^+ ions in the material.

Electrochemical behavior of an electrode material by studying its defect process is important when assessing its use as a possible high-rate electrode material in lithium ion batteries. In particular, the intrinsic lithium ion diffusion in and out of Li_3SbO_4 material with low activation energy is a key requirement its applicability in batteries. Furthermore, the incorporation of additional Li ion in the as prepared Li_3SbO_4 material by doping suitable cations on the Sb site is an efficient way to increase its capacity. In general, it is difficult to derive detailed information about the defects and long range Li ion diffusion paths with activation energies experimentally.

Static atomistic simulation techniques based on the classical pair potentials can provide valuable information on defect process including cation mixing, lithium ion migration paths together with activation energies and doping behaviour to experimentalists to understand the electrochemical behaviour of Li_3SbO_4. This simulation technique has been successfully applied to a various Li and Na ion battery materials[26-32]. For example, the lithium ion diffusion path calculated using atomistic simulation was later confirmed by the neutron

diffraction experment[26]. In our recent study, we have constructuted long range Li ion diffusion paths with low activation energies and proposed that doping by Al on Ti site could increase the Li content in Li_2TiO_3[32]. In the present study we employ atomistic simulation to investigate the relative energetics of the formation of intrinsic defects, the possible pathways for lithium ion conduction and the solution of tetravalent dopants for introducing extra lithium in Li_3SbO_4. DFT calculations were performed to examine the electronic structures of doped and un-doped Li_3SbO_4.

2. Computational Details

Classical pair potential method as implemented in the GULP package[33] was employed to calculate the energetics for the formation of intrinsic defects, possible Li ion diffusion pathways and solution of tetravalent dopants. Classical Born model description of an ionic crystal lattice is adopted in this method. All systems were treated as crystalline solids with interactions between ions consisting of the long-range attractions and short-range repulsive forces representing electron-electron repulsion and van der Waals interactions. Buckingham potentials (refer to Table S1) was used to describe the short range interactions. Broyden-Fletcher-Goldfarb-Shanno (BFGS) algorithm[34]was used to relax simulation boxes and the corresponding atom positions. Lattice relaxation about point defects and the migrating ions was investigated using the Mott-Littleton method[35]. It divides the crystal lattice into two concentric spherical regions, where the ions within the inner spherical region (on the order of >700 ions) immediately surrounding the defect relaxed explicitly. Li ion diffusion was calculated considering two adjacent vacancy sites as initial and final configurations. Seven interstitial Li ions were considered in a direct linear route and they were allowed to relax in x, y, z, xy, yz and xz directions with all other ions. The local maximum energy along this diffusion path is calculated and reported as activation energy of migration. As the present model assumes a full charge ionic model with the calculations corresponding to the dilute limit the defect enthalpies will be overestimated, however, relative energies and trends will be consistent.

In order to investigate the electronic property of doped Li_3SbO_4, the plane wave DFT code CASTEP[36,37] was employed with the plane wave basis set to a cut-off of 450 eV. All of the Li_3SbO_4 supercells were simulated using a 2x2x2 Monkhorst-Pack (MP)[38] k-point grid within a 128-atomic site supercell. Regarding on the exchange and correlation interactions in the crystallographic structure of the material, the formulation with the corrected density functional of Perdew, Burke and Ernzerhof (PBE)[39] is applied in the generalized gradient approximation (GGA) with the use of ultrasoft pseudopotentials.[40] All supercells were

optimized in the minimum energy according to the convergence criteria under constant pressure conditions. The obtained atomic configurations for the doped/undoped and defective supercells were used for the electronic structure calculations. We employ the OPTADOS[41,42] subcode for the Density of States (DOS) investigation as well as the visualization of outputs.

3. Results and discussion

3.1. Crystal Structure of Li_3SbO_4

The crystal structure of Li_3SbO_4 was determined by analogy with Na_3BiO_4. It exhibits a monoclinic crystallographic structure with space group P2/c (lattice parameters a = 5.1578 Å, b = 6.0923 Å, c = 5.1397 Å, α = 90°, β = 108.841° and γ=90°) as reported by Skakle *et al.*[43] Figure 1 shows this structure and the chemical environments of Sb and Li [both forming distorted MO_6 octahedra (M= Li or Sb)]. Initially, experimentally observed monoclinic crystal structure of Li_3SbO_4 was reproduced using classical pair potentials parameters to enable an assessment of the quality and efficacy of these potentials (refer to Table S1 in the supplementary information for the potentials parameters used and method section for the detailed description of the methodology) used in this study. There is a good agreement between the calculated equilibrium lattice constants (tabulated in Table 1) and the lattice constant observed in the experiment.

3.2. Intrinsic defects

We have used classical pair potential simulation to calculate a series of isolated point defect (vacancy and interstitial) energies to determine the formation energies for Frenkel and Schottky-type defects in Li_3SbO_4. These defects are useful to understand the electrochemical behavior of the material. The following equations represent the reactions involving these defects as written using Kröger-Vink notation[44].

$$\text{Li Frenkel: } Li_{Li}^{X} \rightarrow V_{Li}' + Li_i^{\bullet} \quad (1)$$

$$\text{O Frenkel: } O_O^{X} \rightarrow V_O^{\bullet\bullet} + O_i'' \quad (2)$$

$$\text{Sb Frenkel: } Sb_{Sb}^{X} \rightarrow V_{Sb}''''' + Sb_i^{\bullet\bullet\bullet\bullet\bullet} \quad (3)$$

$$\text{Schottky: } 3\,Li_{Li}^{X} + Sb_{Sb}^{X} + 4\,O_O^{X} \rightarrow 3\,V_{Li}' + V_{Sb}''''' + 4\,V_O^{\bullet\bullet} + Li_3SbO_4 \quad (4)$$

$$Li_2O \text{ Schottky: } 2\,Li_{Li}^{X} + O_O^{X} \rightarrow 2\,V_{Li}' + V_O^{\bullet\bullet} + Li_2O \quad (5)$$

$$\text{Li/Sb antisite (isolated): } Li_{Li}^{X} + Sb_{Sb}^{X} \rightarrow Li_{Sb}'''' + Sb_{Li}^{\bullet\bullet\bullet\bullet} \quad (6)$$

$$\text{Li/Sb antisite (cluster): } Li_{Li}^{X} + Sb_{Sb}^{X} \rightarrow \{Li_{Sb}'''' : Sb_{Li}^{\bullet\bullet\bullet\bullet}\}^{X} \quad (7)$$

Reaction energies for these intrinsic defect processes are reported in Figure 2. The most favorable intrinsic disorder is Li Frenkel and the formation of other Frenkel and Schottky defects is unfavourable. The second most favorable defect process is calculated to be the Li-Sb anti-site. This result suggests that there will be a small percentage of Li on Sb sites ($Li_{Sb}^{''''}$) and Sb on Li sites ($Sb_{Li}^{\bullet\bullet\bullet\bullet}$). The exact concentration depends on the temperature and synthetic procedure. Anti-site defect has been observed in a variety of other Li ion battery materials during cycling[16,17,45-48]. The formation enthalpy of Li_2O via the Li_2O Schottky-like reaction (relation 5) is a processes that requires an energy of 3.45 eV per defect (refer to Table S2). This is a process that can lead to further $V_{Li}'$and $V_O^{\bullet\bullet}$ however at elevated temperatures.

The current calculations were performed at 0 K using well-established pair potentials available in the literature. These pair potentials were previously tested and used for calculation at 0 K in various Li ion battery materials using similar simulation code (GULP) (refer to ESI). We anticipate that the formation energies would become slightly lower at room temperature (298 K). As the current potential models may introduce substantial lattice distortion, we have not studied the defects and diffusion processes at different temperatures.

3.3. Lithium ion-diffusion

Lithium ion diffusion with lower activation energy is an essential requirement for a promising high-rate electrode or electrolyte materials in lithium ion batteries. Lithium diffusion paths are often difficult to explore on the atomic scale by experiment alone. However, various possible diffusion paths responsible for lithium ion diffusion can be constructed using static atomistic simulation based on the classical pair potentials. The lithium ion migration path calculated in LiFePO4 using classical pair potentials was exactly observed later in the high-temperature powder neutron diffraction and the maximum entropy method. A curved one-dimensional chain for lithium motion with Li-Li separation of 3.01 Å was clearly visualized along [010] direction in the experiment[26].

For the Li vacancy migration, eight different local Li hops (refer to Figure 3) were calculated. Activation energies are reported in Table 2 together with the Li-Li separation and energy profile diagrams are shown in Figure 4. Long range Li ion diffusion paths connecting local Li hops were constructed. Table 3 summarizes the possible long range paths together with the corresponding overall activation energies. We have considered more long range paths but their overall activation energies were not less than the values reported in the Table 3. We have identified a zig-zag long range path (H→H→H→H)

along *bc* plane (refer to Figure 3) with lower overall activation energy of 0.21 eV. This interesting result shows that this material is expected to be high Li-ion conductor requiring experimental investigation. The second long range path exhibits a zig-zag pattern (D→D→D→D) along *ac* plane with over all activation energy of 0.48 eV. There are no theoretical calculations available in the literature detailing the diffusion mechanism and the migration energies. From a diffusion view point this material can be also considered as an electrolyte. The current investigation needs to be addressed experimentally.

In the current simulation, Li-ion vacancy migration was calculated in the dilute limit. At high concentration of vacancies, migration of phases from single crystal is expected. Such phases can be examined using experimental techniques such as Raman spectroscopy. The current classical potentials used in this study was fitted to the crystals structure of Li_3SbO_4 and valid for defects with dilute concentration. Thus, our current work excluded the migration barrier at high vacancy concentration. Here the activation energy of migration is defined as the position of the highest potential energy along the migration path.

3.4. Tetravalent doping

A promising new electrode or electrolyte material should satisfy the performance demand of high energy density and power density with appropriate safety. Introducing extra lithium into the as-prepared material will enhance the capacity and further increase the applicability of Li_3SbO_4 as an electrode or electrolyte material for rechargeable lithium batteries. A possible engineering strategy to increase the concentration of lithium is by doping tetravalent cations on Sb site through creating Li interstitials. Kuganathan *et al.*[19] have used similar approach in their computational studies in Li_2MnSiO_4 cathode material and demonstrated that subvalent doping Al on the Si site could be a synthesis strategy to increase the Li content. Here we considered the solution of RO_2 (*R* = Si, Ge, Ti, Zr and Ce) via the following process (in Kröger-Vink notation) and calculated solution energies using classical pair potential simulation.

$$2\,RO_2 + 2Sb_{Sb}^{X} + Li_2O \rightarrow 2\,R'_{Sb} + 2\,Li_i^{\bullet} + Sb_2O_5 \qquad (8)$$

Solution energies of RO_2 is reported in Figure 5. The results reveal that the most favorable dopant solution energy (0.15 eV) is calculated for SiO_2. This suggests that a possible synthesis-doping strategy of introducing additional lithium into Li_3SbO_4 is by doping Si^{4+} on Sb site, although the exact amount of Si incorporation cannot be predicted. The possible composition of Si-doped Li_3SbO_4 would be $Li_{3+x}Sb_{1-x}Si_xO_4$ (x= 0.0 – 1.0). The second most

favorable dopant is Ti^{4+} with the solution energy of 0.27 eV. The solution energy for ZrO_2 is only 0.09 eV higher than that of TiO_2. Solution energy for CeO_2 is highly endothermic.

Local coordination of Sb with oxygen together with bond lengths and angles in the relaxed structure of undoped Li_3SbO_4 and the dopants occupying Sb site are reported in Figure 6. The ionic radius of Sb^{5+} in octahedral coordination is 0.60 Å. The ionic radius of Si^{4+} is 0.40 Å smaller than that of Sb^{5+}. In the SiO_6 unit, four Si-O bonds are shorter compared to the Sb-O bonds present in the undoped Li_3SbO_4 and the other R-O bonds. This is due to its smaller cation size of Si^{4+} which strongly polarises the oxygen ions forming strong bonds with O atoms. The second lowest solution energy (0.27 eV) is found for Ti^{4+}. Its ionic radius (0.605 Å) is very close to the radius of Sb^{5+}. However, due to its relatively smaller charge (+4), the solution energy slightly increases. Bigger size of the Zr^{4+}compared to that of Si^{4+} shows a higher solution energy. This is reflected in longer bond lengths of Zr-O and shorter bond angles. There is a significant rise in the solution energy (2.30 ev) for CeO_2 due to its larger ionic radius reflecting in the longest bond lengths and shortest angles. The ionic radius of Ge^{4+} (0.53 Å) which is smaller than that of Ti^{4+} or Sb^{5+} and larger than that of Si^{4+}. The solution energy (0.64 eV) is higher than that of Si^{4+}, Ti^{4+} and Zr^{4+} The exact reason for the higher solution energy should be due to other factors.

3.5. Electronic structures of dopants

For the tetravalent dopants considered we have used DFT and have employed density of states (DOS) calculations to consider the contribution of every element (partial-DOS). In Figure 7. the PDOS for the (a) Li_3SbO_4 perfect cell (b) Li_3SbO_4 with a Li vacancy (c) Si – Doped Li_3SbO_4 and (d) Si- Doped Li_3SbO_4 with Li vacancy. Overall, the formation profile of the electronic structure indicates the ionic conduction to be the dominant mechanism as compared to the electronic. The valence band maximum (VBM) is at zero energy level with the band gap being approx. 6 eV. However, an additional in – gap contribution is observed at 2.58 eV from the valence band with a width of 2.03 eV as presented in Fig 7(a). Due to this non-continuation we are not counting the intermediate contribution as a part of the conduction band. The electronic structure is characterized by the O^{2-} p-states near the Fermi level whereas the edge of the conduction band is characterized by the Sb^{5+} p-states and Li^{+} p-states as well. (Refer to Figure S1 of ESI) All elements are present to the in-gap contribution indicating a type of anisotropy for the electronic properties. Furthermore, the presence of Li^{+} vacancies in the crystal do not affect the PDOS profile as shown in Fig 7 (b). In terms of the doping effect, additional states for all cases appear as a consequence of the

substitutional atom that resides on the Sb^{5+} site. Interestingly the intensity as well as the quantity of these states increase with the ionic radius of the dopant (Refer to Figure 2 of SI). The Si case that corresponds to the lower radius and solution enthalpy of the system, presents the lowest contribution as shown in Fig 7 (c). In accordance with the un-doped supercell, no considerable changes are observed to the total DOS with the formation of a Li^+ vacancy. However, for bigger ions there is an increasing amount of extra states with Zr and Ce to be the most representative cases.

4. Conclusion

Atomistic simulation techniques have been used in this study to investigate the intrinsic defects, lithium ion mobility and tetravalent doping, which are relevant to the general electrochemical behavior of Li_3SbO_4 as a lithium battery electrode material. The dominant energy defect process is Li Frenkel. The Li/Sb anti-site energies suggest that there would be no significant intrinsic concentration of Sb on Li sites at operating temperatures in Li_3SbO_4. Investigation of the Li ion diffusion paths in Li_3SbO_4 indicates relatively low migration energy (0.21eV) along *bc* plane with a zig-zag pattern, suggesting high Li mobility, which is important for good rate capability and capacity retention. We have considered the solution energies of RO_2 (R = Si, Ge, Ti, Zr and Ce) to create extra lithium in this material and found that SiO_2 has the lowest solution energy. This interesting results presented here demonstrate that future experimental work should be stimulated on this important lithium ion battery material. The introduction of tetravalent dopants will not alter the band-gap significantly.

Conflicts of interest

The authors declare that there is no competing financial interest.

Acknowledgement

Computational facilities and support were provided by High Performance Computing Centre at Imperial College London and Coventry University.

References

1 J. M. Tarascon and M. Armand, *Nature*, 2001, 414, 359.

2 M. Armand and J. M. Tarascon, *Nature*, 2008, 451, 652.

3 N. Kamaya, K. Homma, Y. Yamakawa, M. Hirayama, R. Kanno, M. Yonemura, T. Kamiyama, Y. Kato, S. Hama, K. Kawamoto and A. Mitsui, *Nat. Mater*, 2011, 10, 682.

4 Y. Zhao and L. L. Daemen, *J. Am. Chem. Soc*, 2012, 134, 15042-15047.

5 P. G. Bruce, S. A. Freunberger, L. J. Hardwick and J.-M. Tarascon, *Nat. Mater*, 2011, 11, 19.

6 E. E. Jay, M. J. D. Rushton, A. Chroneos, R. W. Grimes and J. A. Kilner, *Phys. Chem. Chem. Phys* , 2015, 17, 178-183.

7 D. O. Shin, K. Oh, K. M. Kim, K.-Y. Park, B. Lee, Y.-G. Lee and K. Kang, *Sci. Rep*, 2015, 5, 18053.

8 M. Klenk and W. Lai, *Phys. Chem. Chem. Phys*, 2015, 17, 8758-8768.

9 C. A. J. Fisher, N. Kuganathan and M. S. Islam, *J. Mater. Chem. A*, 2013, 1, 4207-4214.

10 Y. Kato, S. Hori, T. Saito, K. Suzuki, M. Hirayama, A. Mitsui, M. Yonemura, H. Iba and R. Kanno, *Nat. Energy*, 2016, 1, 16030.

11 C. Chen, Z. Lu and F. Ciucci, *Sci. Rep*, 2017, 7, 40769.

12 X. He, Y. Zhu and Y. Mo, *Nat. Commun*, 2017, 8, 15893.

13 A. K. Padhi, K. S. Nanjundaswamy and J. B. Goodenough, *J. Electrochem. Soc*, 1997, 144, 1188-1194.

14 A. Nytén, A. Abouimrane, M. Armand, T. Gustafsson and J. O. Thomas, *Electrochem. Commun*, 2005, 7, 156-160.

15 S.-i. Nishimura, S. Hayase, R. Kanno, M. Yashima, N. Nakayama and A. Yamada, *J. Am. Chem. Soc*, 2008, 130, 13212-13213.

16 A. R. Armstrong, N. Kuganathan, M. S. Islam and P. G. Bruce, *J. Am. Chem. Soc.*, 2011, 133, 13031-13035.

17 V. V. Politaev, A. A. Petrenko, V. B. Nalbandyan, B. S. Medvedev and E. S. Shvetsova, *J. Solid State Chem*, 2007, 180, 1045-1050.

18 R. Dominko, M. Bele, M. Gaberščček, A. Meden, M. Remškar and J. Jamnik, *Electrochem. Commun*, 2006, 8, 217-222.

19 N. Kuganathan and M. S. Islam, *Chem. Mater*, 2009, 21, 5196-5202.

20 S.-i. Nishimura, M. Nakamura, R. Natsui and A. Yamada, *J. Am. Chem. Soc*, 2010, 132, 13596-13597.

21 S. Afyon, M. Wörle and R. Nesper, *Angew. Chemie Inter. Ed.*, 2013, 52, 12541-12544.

22 K. Mizushima, P. C. Jones, P. J. Wiseman and J. B. Goodenough, *Mater. Res. Bull*, 1980, 15, 783-789.

23 Q. Jacquet, G. Rousse, A. Iadecola, M. Saubanère, M.-L. Doublet and J.-M. Tarascon, *Chem. Mater*, 2018, 30, 392-402.

24 M. Kundu, S. Mahanty and R. N. Basu, *Mater. Lett*, 2011, 65, 1105-1107.

25 M. Kundu, S. Mahanty and R. N. Basu, *Mater. Lett*, 2011, 65, 3083-3085.

26 M. S. Islam, D. J. Driscoll, C. A. J. Fisher and P. R. Slater, *Chem. Mater* , 2005, 17, 5085-5092.

27 N. Kuganathan, P. Iyngaran and A. Chroneos, *Sci. Rep*., 2018, 8, 5832.

28 A. Kordatos, N. Kuganathan, N. Kelaidis, P. Iyngaran and A. Chroneos, *Sci. Rep*., 2018, 8, 6754.

29 N. Kuganathan, S. Ganeshalingam and A. Chroneos, *Sci. Rep*, 2018, 8, 8140.

30 N. Kuganathan, A. Kordatos and A. Chroneos, *Sci. Rep*, 2018, 8, 12621.

31 N. Kuganathan and A. Chroneos, *Sci. Rep*, 2018, 8, 14669.

32 N. Kuganathan, A. Kordatos, M. E. Fitzpatrick, R. V. Vovk and A. Chroneos, *Solid State Ionics*, 2018, 327, 93-98.

33 J. D. Gale and A. L. Rohl, *Molec. Simul*, 2003, 29, 291-341.

34 J. D. Gale, *J. Chem. Soc. Faraday Trans.*, 1997, 93, 629-637.

35 N. F. Mott and M. J. Littleton, *Trans. Faraday Soc*, 1938, 34, 485-499.

36 M. C. Payne, M. P. Teter, D. C. Allan, T. A. Arias and J. D. Joannopoulos, *Rev. Mod. Phys.*, 1992, 64, 1045-1097.

37 M. D. Segall, J. D. L. Philip, M. J. Probert, C. J. Pickard, P. J. Hasnip, S. J. Clark and M. C. Payne, *J. Phys. Condens. Matter*, 2002, 14, 2717.

38 H. J. Monkhorst and J. D. Pack, *Phys. Rev. B* , 1976, 13, 5188-5192.

39 J. P. Perdew, K. Burke and M. Ernzerhof, *Phys. Rev. Lett*, 1996, 77, 3865-3868.

40 D. Vanderbilt, *Phys. Rev. B*, 1990, 41, 7892-7895.

41 R. J. Nicholls, A. J. Morris, C. J. Pickard and J. R. Yates, *J. Phys.: Conf. Ser* , 2012, 371, 012062.

42 A. J. Morris, R. J. Nicholls, C. J. Pickard and J. R. Yates, *Comp. Phys. Comm* , 2014, 185, 1477-1485.

43 J. M. S. Skakle, M. A. Castellanos R, S. T. Tovar, S. M. Fray and A. R. West, *J. Mater. Chem*, 1996, 6, 1939-1942.

44 F. A. Kröger and H. J. Vink, in *Solid State Physics*, eds. F. Seitz and D. Turnbull, Academic Press, 1956, vol. 3, pp. 307-435.

45 A. Nytén, S. Kamali, L. Häggström, T. Gustafsson and J. O. Thomas, *J. Mater. Chem*, 2006, 16, 2266-2272

46 D. Ensling, M. Stjerndahl, A. Nytén, T. Gustafsson and J. O. Thomas, *J. Mater. Chem*, 2009, 19, 82-88.

47 H. Liu, M.-J. Choe, R. A. Enrique, B. Orvañanos, L. Zhou, T. Liu, K. Thornton and C. P. Grey, *Phys. Chem C*, 2017, 121, 12025-12036.

48 M. Kempaiah Devaraju, Q. Duc Truong, H. Hyodo, Y. Sasaki and I. Honma, *Sci. Rep* , 2015, 5, 11041.

Table 1. Calculated and Experimental Structural Parameters for monoclinic (P2/c) Li_3SbO_4

Parameter	Calc	Expt [43]	|Δ|(%)
a (Å)	5.1406	5.1578	0.33
b (Å)	6.1999	6.0923	1.77
c (Å)	5.0877	5.1397	1.01
α (°)	90.0	90.0	0.00
β (°)	107.716	108.841	1.03
γ (°)	90.0	90.0	0.00

Table 2. Calculated Li-Li separations and activation energies for the lithium ion migration between two adjacent Li sites (refer to Figure 3).

Migration path	Li-Li separation (Å)	Activation energy (eV)
A	2.963	0.69
B	2.554	0.19
C	3.646	1.09
D	2.787	0.41
E	3.027	0.56
F	2.832	0.67
G	3.021	0.60
H	2.703	0.21

Table 3. Possible long range Li ion diffusion paths and their corresponding overall activation energies.

Long range path	Overall activation energy (eV)
A→A→A→A	0.69
B→C→B→C	1.09
D→D→D→D	0.41
E→E→E→E	0.56
F→F→F→F	0.67
G→G→G→G	0.60
H→H→H→H	0.21

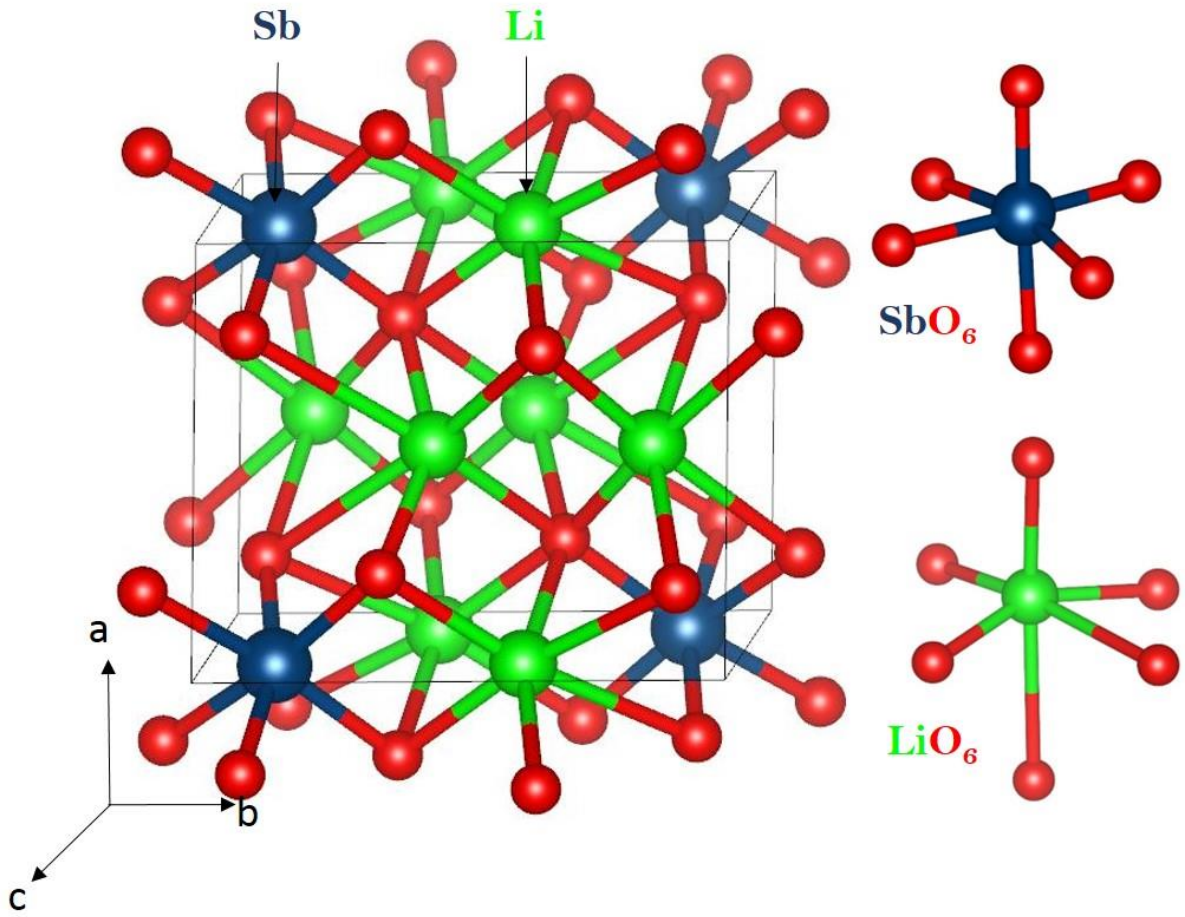

Figure 1. Crystal structure of Li_3SbO_4 (space group P2/c)

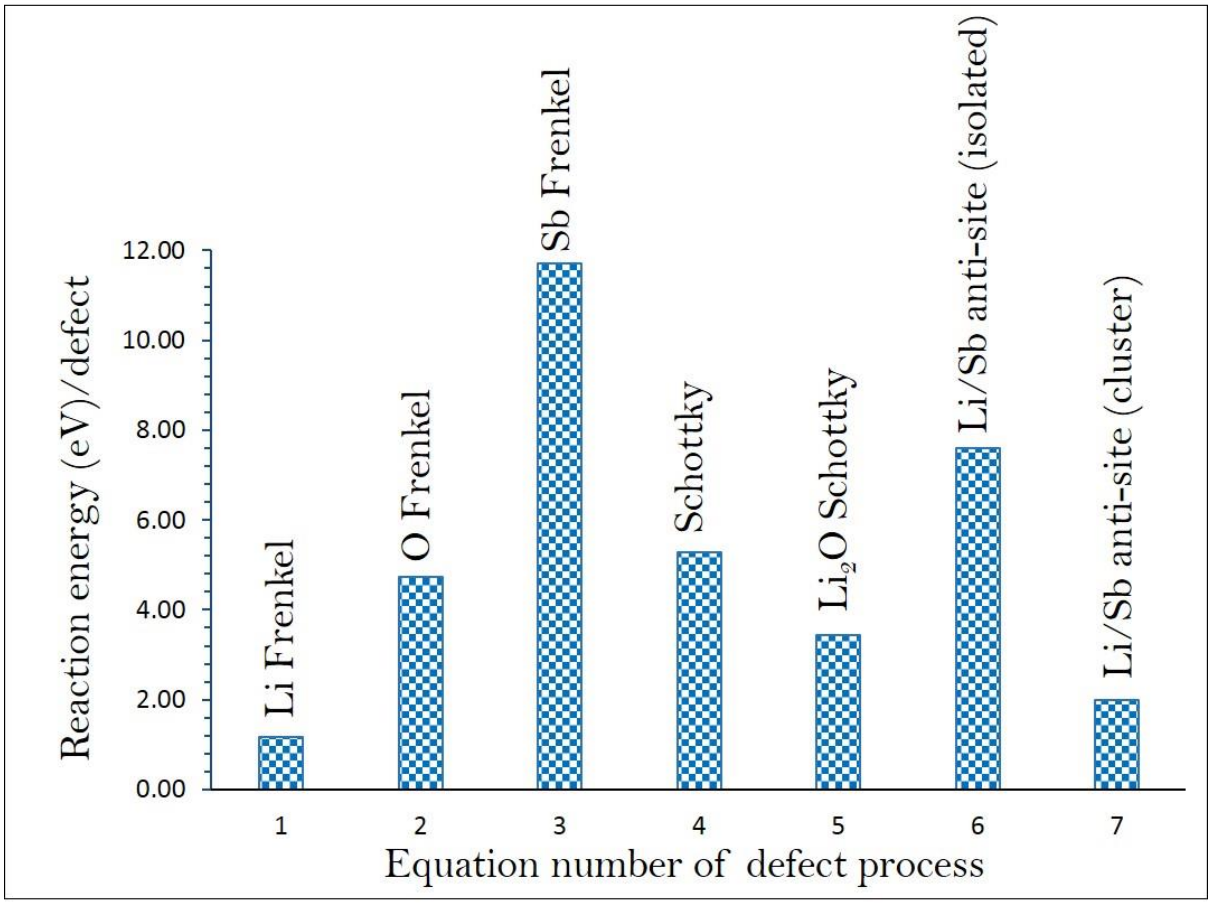

Figure 2. Energetics of intrinsic defect process in monoclinic Li_3SbO_4.

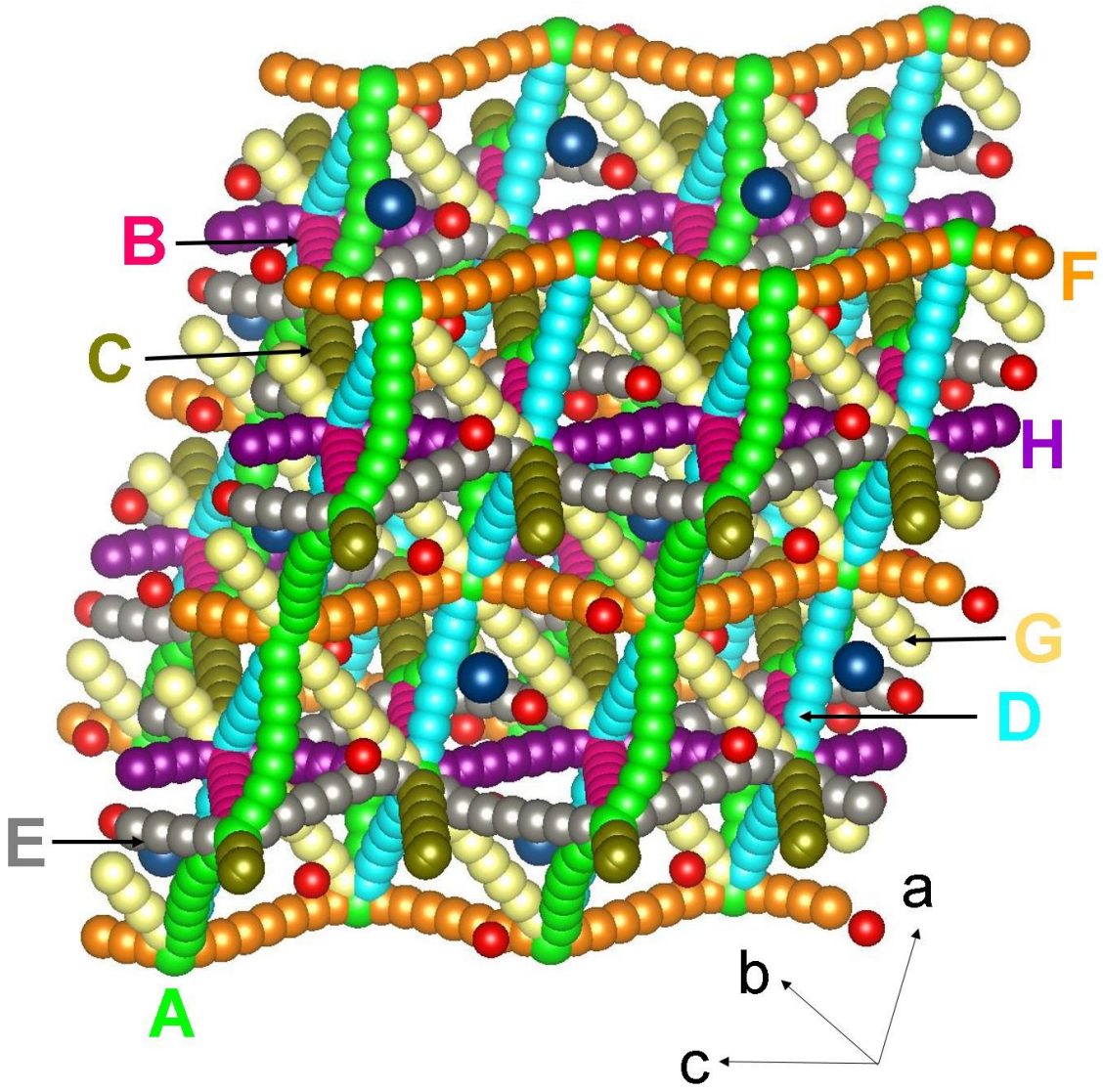

Figure 3. Possible long range lithium vacancy migration paths considered. Local Li migration paths are shown in eight different colors. Blue and red colors correspond to Sb and O atoms respectively.

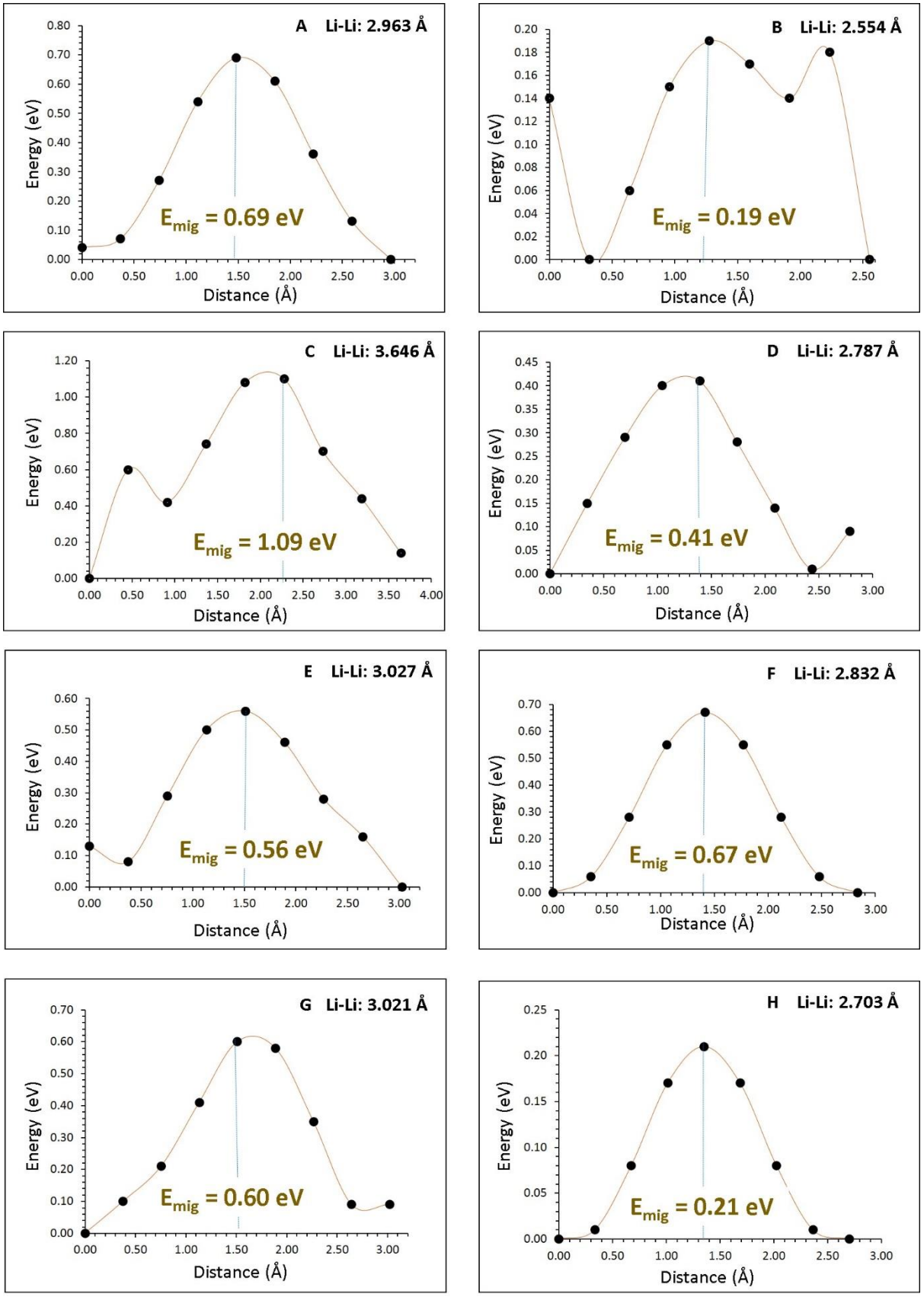

Figure 4. Eight different energy profiles [as shown in Figure 3] of Li vacancy hopping between two adjacent Li sites in Li_3SbO_4.

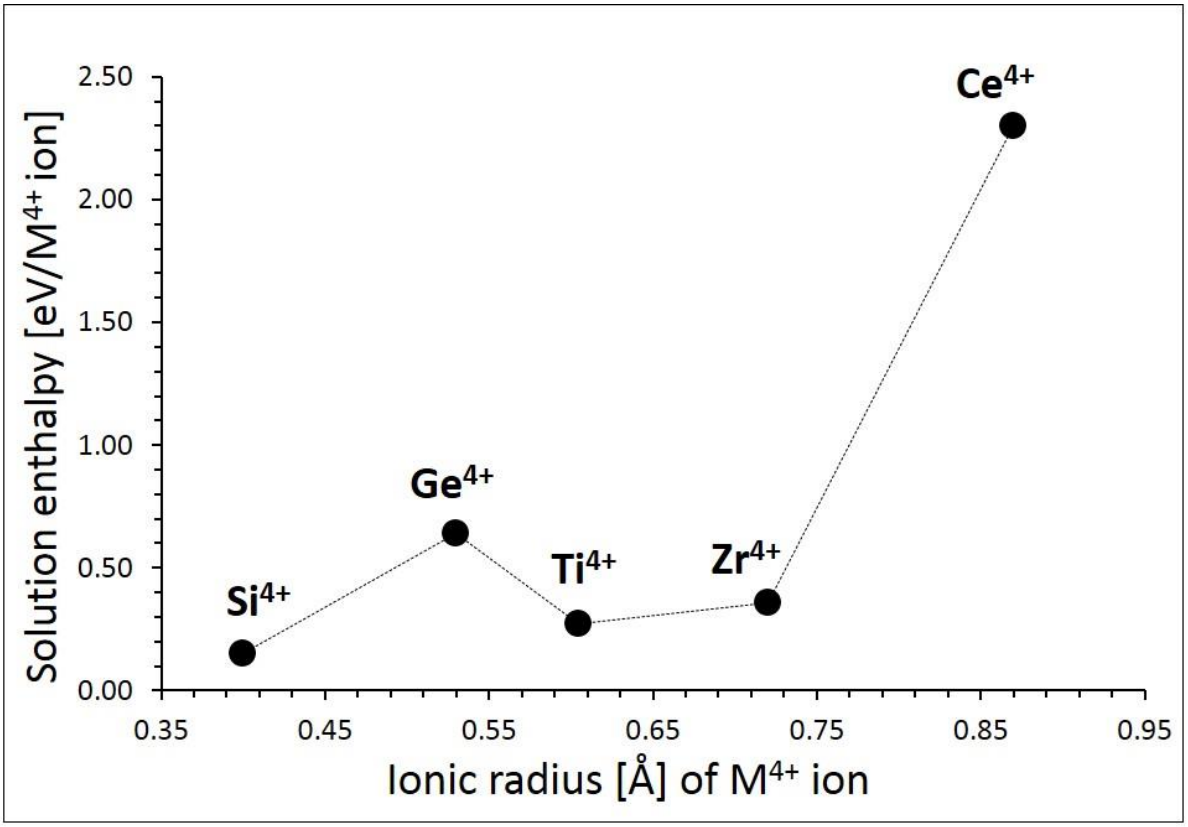

Figure 5. Enthalpy of solution of RO_2 (R = Si, Ge, Ti, Zr, Gd and Ce) with respect to the R^{4+} ionic radius in Li_3SbO_4.

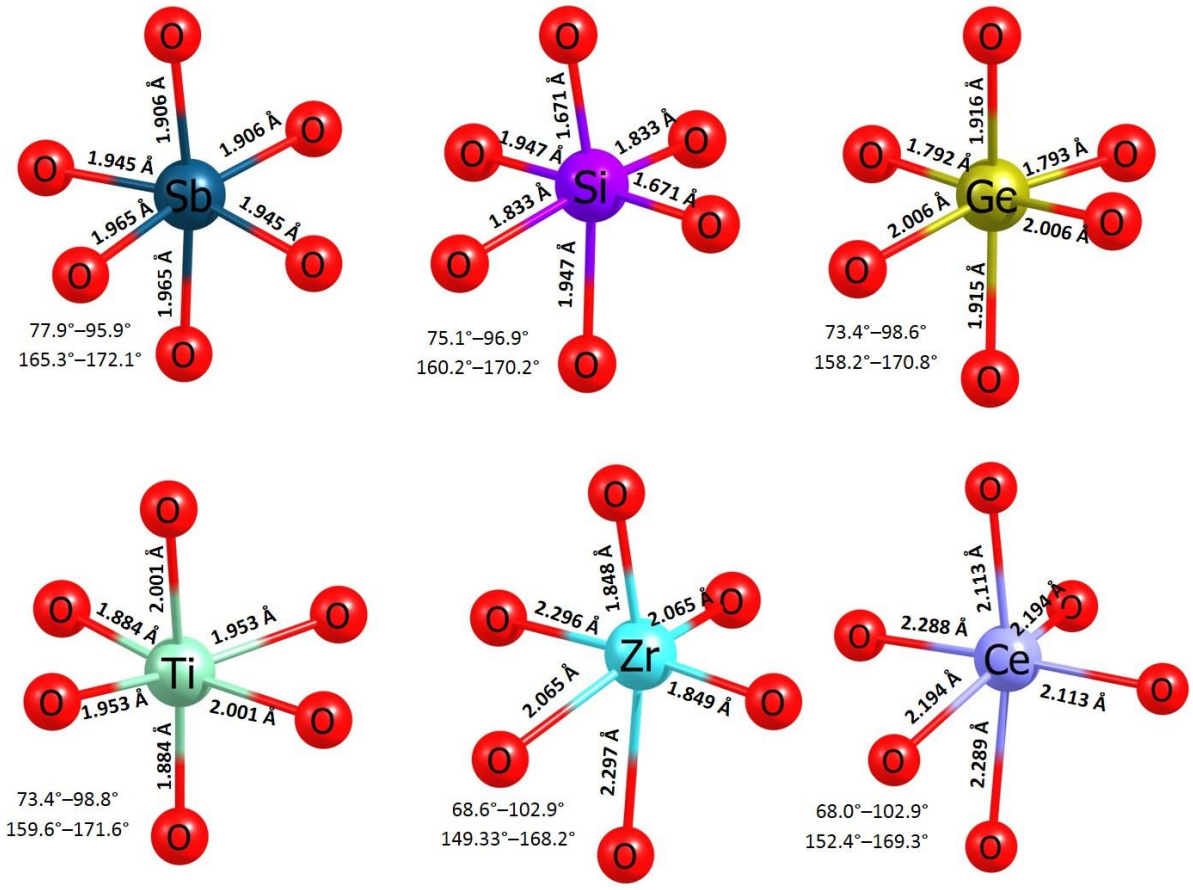

Figure 6. Octahedral SbO_6 unit in the relaxed structure of un-doped Li_3SbO_4 and the coordination formed by the dopants on the Sb site with neighbor oxygen.

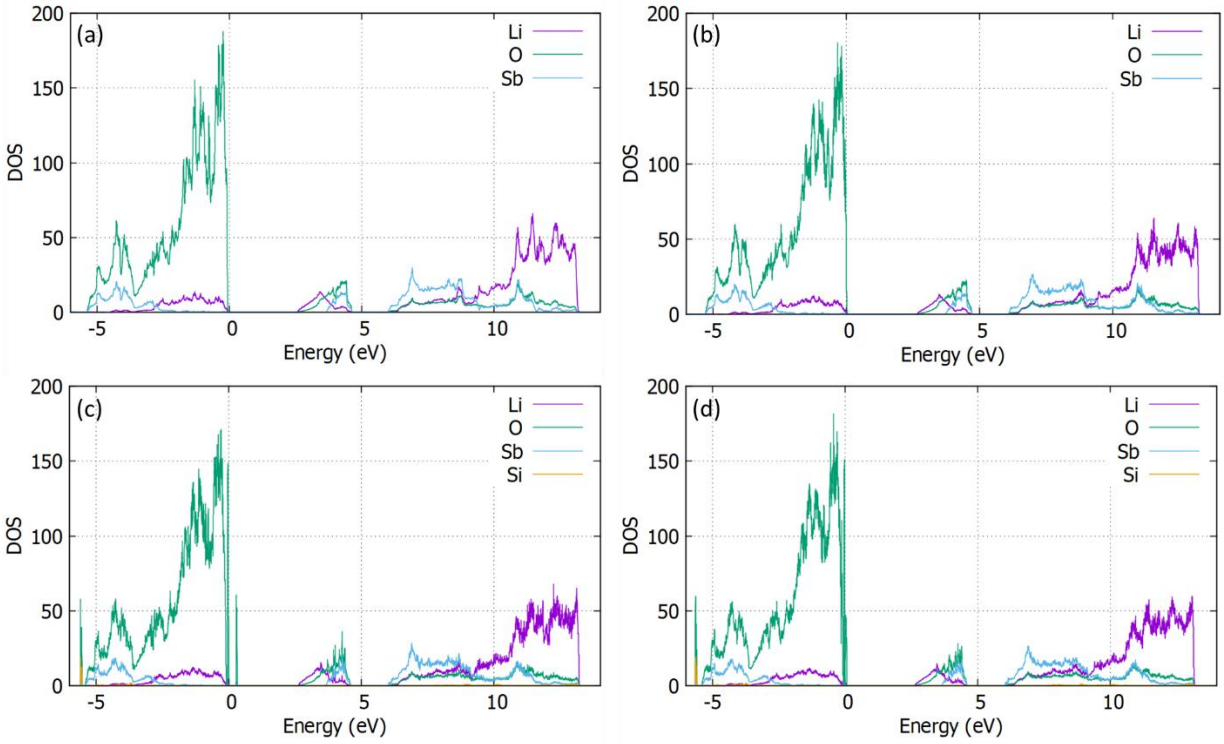

Figure 7. The PDOS for the (a) Li_3SbO_4 perfect cell (b) Li_3SbO_4 with a Li vacancy (c) Si – Doped Li_3SbO_4 and (d) Si- Doped Li_3SbO_4 with Li vacancy.